

NLO QCD corrections to B_c -pair production in photon-photon collisions

Zi-Qiang Chen^{1,†}, Hao Yang^{1,‡} and Cong-Feng Qiao^{1,2,*}

¹*School of Physics, University of Chinese Academy of Science, Yuquan Road 19A, Beijing 10049, China*

²*CAS Key Laboratory of Vacuum Physics, Beijing 100049, China*



(Received 19 May 2020; accepted 6 July 2020; published 16 July 2020)

The B_c meson pair, including pairs of pseudoscalar states and vector states, productions in high energy photon-photon interaction are investigated at the next-to-leading order (NLO) accuracy in the non-relativistic quantum chromodynamics factorization formalism. The corresponding cross sections at the future e^+e^- colliders with $\sqrt{s} = 250$ GeV and 500 GeV are evaluated. Numerical result indicates that the inclusion of the NLO corrections shall greatly suppress the scale dependence and enhance the prediction reliability. In addition to the phenomenological meaning, the NLO QCD calculation of this process subjects to certain technical issues, which are elucidated in detail and might be applicable to other relevant investigations.

DOI: [10.1103/PhysRevD.102.016011](https://doi.org/10.1103/PhysRevD.102.016011)

I. INTRODUCTION

As the only heavy meson consisting of two heavy quarks with different flavors, the B_c meson is of great interest in both experiment and theory. The study of its production and decays may enrich our knowledge on the properties of double heavy meson and the nature of perturbative QCD (pQCD). The ground state of B_c meson, $B_c^+(1S)$, was discovered by CDF Collaboration [1,2] in 1998. And its excited state $B_c^+(2S)$ was observed by ATLAS [3] and CMS [4] Collaborations in 2014 and 2019, respectively.

Due to the large masses of bottom and charm quarks, the production of heavy quark pair can be described by pQCD, while the hadronization process can be factored by using the NRQCD factorization formalism [5]. For inclusive B_c meson production, various investigations have been carried out, including the direct production through pp [6–9], e^+e^- [10,11], $\gamma\gamma$ [12,13], and ep [14,15] collisions, and the indirect production through top quark [16,17], Z boson [18–21], W boson [22–24], and Higgs boson [25] decays.

Within QCD and quantum electromagnetic dynamics, the B_c^+ meson is produced in accompany with an additional $b\bar{c}$ pair, which is also possible to form another $b\bar{c}$ meson, namely, the B_c pair may exclusively be produced. Generally speaking, the experiment measurement of

exclusive process possesses a relative high precision, which is required in exploring the properties of QCD and hadrons. In the literature, various B_c -pair production processes have been investigated, including in pp [26,27], e^+e^- [28–30], and $\gamma\gamma$ [26] collisions. We notice that in Ref. [26] the leading order (LO) analysis on B_c -pair production in photon-photon collision was performed, however with only $B_c^+ + B_c^-$ (pseudoscalar-pseudoscalar, PP) and $B_c^{*+} + B_c^{*-}$ (vector-vector, VV) configurations being considered. In this work, for the sake of completeness, we first repeat the LO calculation in [26] and then calculate the LO B_c -pair production in $B_c^+ + B_c^-$ (pseudoscalar-vector, PV) and $B_c^{*+} + B_c^-$ (vector-pseudoscalar, VP) configurations.¹ In the end, all these processes will be evaluated up to the next-to-leading order (NLO) QCD accuracy. Note, hereafter for simplicity, B_c represents for both pseudoscalar B_c and vector B_c^* , the latter may overwhelmingly decay to the pseudoscalar state, unless specifically mentioned.

The rest of the paper is organized as follows. In Sec. II, we present the primary formulas employed in the calculation. In Sec. III, some technical details in the analytical calculation are given. In Sec. IV, the numerical evaluation for concerned processes is performed. The last section is remained for summary.

II. FORMULATION

According to NRQCD factorization formalism, the cross section of B_c -pair production via photon-photon fusion can be formulated as

¹The production of PV and VP is related by a charge-conjugation transformation. Their cross section is exactly the same.

* Corresponding author.

qiaocf@ucas.ac.cn

† chenziqiang13@mails.ucas.ac.cn

‡ yanghao174@mails.ucas.ac.cn

Published by the American Physical Society under the terms of the Creative Commons Attribution 4.0 International license. Further distribution of this work must maintain attribution to the author(s) and the published article's title, journal citation, and DOI. Funded by SCOAP³.

$$d\hat{\sigma}(\gamma + \gamma \rightarrow B_c^+ + B_c^-) = \frac{|\psi(0)|^4}{2\hat{s}} \frac{1}{4} \sum |\mathcal{M}(\gamma + \gamma \rightarrow [c\bar{b}] + [b\bar{c}])|^2 d\text{PS}_2, \quad (1)$$

where $\psi(0)$ is the wave function of B_c meson at the origin, \hat{s} is the center-of-mass energy square of two colliding photons, \sum sums over the polarizations and colors of the initial and final particles, $\frac{1}{4}$ comes from the spin average of the initial $\gamma\gamma$ states, $\mathcal{M}(\gamma + \gamma \rightarrow [c\bar{b}] + [b\bar{c}])$ is the corresponding partonic amplitude, and $d\text{PS}_2$ stands for the two-body phase space.

The partonic amplitude can be computed by using the covariant projection operator method. At the leading order of the relative velocity expansion, it is legitimate to take $m_{B_c} = m_b + m_c$, $p_{B_c} = p_c + p_b = (1 + \frac{m_c}{m_b})p_b$. The spin and color projection operator has the form

$$\Pi(n) = \frac{1}{2\sqrt{m_{B_c}}} \epsilon(n) (\not{p}_{B_c} + m_{B_c}) \otimes \left(\frac{1_c}{\sqrt{N_c}} \right), \quad (2)$$

where $\epsilon(^1S_0) = \gamma_5$, $\epsilon(^3S_1) = \not{\epsilon}$, and ϵ represents the polarization vector of B_c^* meson. The 1_c stands for the unit color matrix and $N_c = 3$ for the number of colors in QCD.

The photon-photon scattering may be achieved in high energy e^+e^- collider like the Large Electron-Positron Collider, the Circular Electron Positron Collider (CEPC), and the International Linear Collider (ILC), or even in hadron collider like the Large Hadron Collider. Here we focus only on the e^+e^- collision case, where the initial photon can be generated by the bremsstrahlung or by the laser backscattering (LBS) effect. The cross section is then formulated as

$$d\sigma(e^+ + e^- \rightarrow e^+ + e^- + B_c^+ + B_c^-) = \int dx_1 dx_2 f_\gamma(x_1) f_\gamma(x_2) d\sigma(\gamma + \gamma \rightarrow B_c^+ + B_c^-), \quad (3)$$

where $f_\gamma(x)$ is the photon distribution with fraction x of the beam energy.

Imposing transverse momentum cut $p_T^- < p_T < p_T^+$ and rapidity cut $|y| < y_c$ on each B_c meson, the formula for total cross section is then

$$\begin{aligned} \sigma(e^+ + e^- \rightarrow e^+ + e^- + B_c^+ + B_c^-) &= \frac{1}{256\pi} \left\{ \theta \left(-\ln \frac{2m_T^-}{\sqrt{s}} \right) \int_{\ln \frac{2m_T^-}{\sqrt{s}}}^{\min\{0, \ln \frac{2m_T^+}{\sqrt{s}}\}} dX \int_{\max\{-y_T^+, -y_c\}}^{\min\{y_T^+, y_c\}} dy^* \frac{\text{sech}^2 y^*}{E_1^2} \sum |\mathcal{M}|^2 \right. \\ &\quad \times \int_{\max\{-y_c + y^*, X\}}^{\min\{y_c - y^*, -X\}} dy_0 x_1 f_\gamma(x_1) x_2 f_\gamma(x_2) + \theta \left(-\ln \frac{2m_T^+}{\sqrt{s}} \right) \int_{\ln \frac{2m_T^+}{\sqrt{s}}}^{\min\{0, \ln(\frac{2m_T^+}{\sqrt{s}} \cosh y_c)\}} dX \\ &\quad \times \left(\int_{y_T^-}^{\min\{y_T^+, y_c\}} dy^* + \int_{\max\{-y_T^+, -y_c\}}^{-y_T^-} dy^* \right) \frac{\text{sech}^2 y^*}{E_1^2} \sum |\mathcal{M}|^2 \\ &\quad \left. \times \int_{\max\{-y_c + y^*, X\}}^{\min\{y_c - y^*, -X\}} dy_0 x_1 f_\gamma(x_1) x_2 f_\gamma(x_2) \right\}, \quad (4) \end{aligned}$$

with

$$\begin{aligned} X &= \frac{1}{2} \ln(x_1 x_2), \quad y_0 = \frac{1}{2} \ln \frac{x_1}{x_2}, \\ m_T^\pm &= \sqrt{m_{B_c}^2 + p_T^{\pm 2}}, \\ y_T^\pm &= \frac{1}{2} \ln \frac{E_1 + \sqrt{E_1^2 - m_T^{\mp 2}}}{E_1 - \sqrt{E_1^2 - m_T^{\mp 2}}}. \quad (5) \end{aligned}$$

Here, \sqrt{s} is the collision energy of e^+e^- collider, $E_1 = \sqrt{s x_1 x_2}/2$, and $y^* = y - y_0$ are, respectively, the energy and rapidity of B_c meson in the photon-photon center-of-mass system; $\theta(x)$ means the unit step function.

The spectrum of bremsstrahlung photon is well formulated in the Weizsacker-Williams approximation (WWA) as [31]

$$f_\gamma(x) = \frac{\alpha}{2\pi} \left[\frac{1 + (1-x)^2}{x} \log \left(\frac{Q_{\max}^2}{Q_{\min}^2} \right) + 2m_e^2 x \left(\frac{1}{Q_{\max}^2} - \frac{1}{Q_{\min}^2} \right) \right], \quad (6)$$

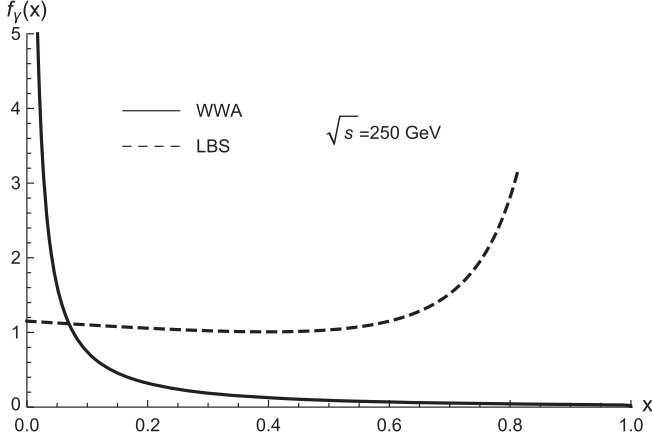


FIG. 1. The spectra of WWA photon and LBS photon at $\sqrt{s} = 250$ GeV.

where $Q_{\min}^2 = m_e^2 x^2 / (1-x)$ and $Q_{\max}^2 = Q_{\min}^2 + (\theta_c \sqrt{s}/2)^2 (1-x)$ with $x = E_\gamma/E_e$, θ_c is the experimental angular cut which is taken to be 32 mrad here. For the LBS photon, the spectrum is expressed as [32]

$$f_\gamma(x) = \frac{1}{N} \left[1 - x + \frac{1}{1-x} - 4r(1-r) \right], \quad (7)$$

where $r = \frac{x}{x_m(1-x)}$ and the normalization factor

$$N = \left(1 - \frac{4}{x_m} - \frac{8}{x_m^2} \right) \log(1+x_m) + \frac{1}{2} + \frac{8}{x_m} - \frac{1}{2(1+x_m)^2}. \quad (8)$$

Here, $x_m \simeq 4.83$ [33] and the energy fraction x of photon is restricted in $0 \leq x \leq x_m/(1+x_m)$. The behaviors of WWA photon and LBS photon are quite different; their spectra at $\sqrt{s} = 250$ GeV are shown in Fig. 1.

III. ANALYTICAL CALCULATION

The typical tree-level and one-loop Feynman diagrams for the partonic processes are shown in Fig. 2. The momenta and the polarization vectors of incoming and outgoing particles are denoted as

$$\gamma(p_1, \epsilon_1) + \gamma(p_2, \epsilon_2) \rightarrow [c\bar{b}](k_1, \epsilon_3) + [\bar{c}b](k_2, \epsilon_4). \quad (9)$$

Here, initial and final state particles are all on their mass shells $p_1^2 = p_2^2 = 0$ and $k_1^2 = k_2^2 = m_{B_c}^2$. The polarization vectors satisfy the constraints $\epsilon_1 \cdot \epsilon_1^* = \epsilon_2 \cdot \epsilon_2^* = \epsilon_3 \cdot \epsilon_3^* = \epsilon_4 \cdot \epsilon_4^* = -1$ and $p_1 \cdot \epsilon_1 = p_2 \cdot \epsilon_2 = k_1 \cdot \epsilon_3 = k_2 \cdot \epsilon_4 = 0$.

To proceed the calculation, we notice working in the photon-photon center-of-mass system is convenient. By introducing the orthonormal four-vector base: $n_0 = (1, 0, 0, 0)$, $n_1 = (0, 1, 0, 0)$, $n_2 = (0, 0, 1, 0)$, and $n_3 = (0, 0, 0, 1)$, we may choose

$$\begin{aligned} p_1 &= E_1(n_0 + n_3), & p_2 &= E_1(n_0 - n_3), \\ k_1 &= E_1(n_0 + r_y n_2 + r_z n_3), & k_2 &= E_1(n_0 - r_y n_2 - r_z n_3) \end{aligned} \quad (10)$$

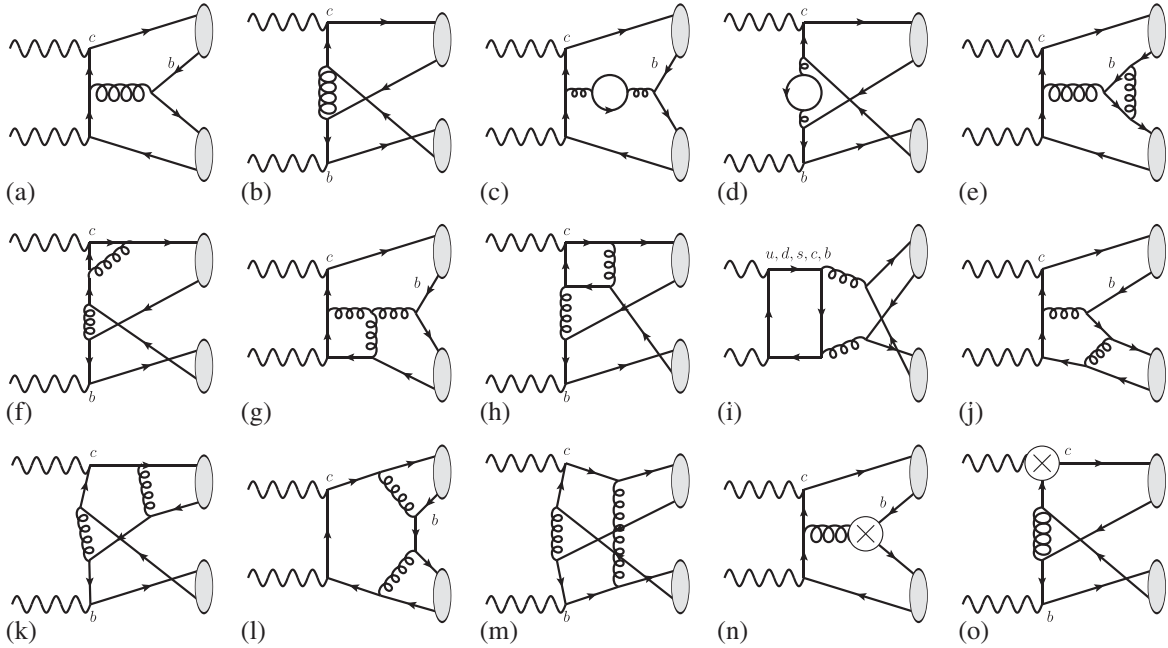


FIG. 2. Typical Feynman diagrams of the partonic processes for B_c -pair production. (a),(b) Tree-level diagrams. (c),(d) Self-energy corrections. (e),(f) Vertex corrections. (g)–(i) Box diagrams. (j),(k) Pentagon diagrams. (l),(m) Hexagon diagrams. (n),(o) Diagrams of counterterms.

$$\begin{aligned}
 \epsilon_1^{(1)} &= n_1, & \epsilon_1^{(2)} &= n_2, & \epsilon_2^{(1)} &= n_1, & \epsilon_2^{(2)} &= n_2, \\
 \epsilon_3^{(1)} &= n_1, & \epsilon_3^{(2)} &= \frac{r_z n_2 - r_y n_3}{\sqrt{r_y^2 + r_z^2}}, & \epsilon_3^{(3)} &= \frac{(r_y^2 + r_z^2)n_0 + r_y n_2 + r_z n_3}{r_m \sqrt{r_y^2 + r_z^2}}, \\
 \epsilon_4^{(1)} &= n_1, & \epsilon_4^{(2)} &= \frac{r_z n_2 - r_y n_3}{\sqrt{r_y^2 + r_z^2}}, & \epsilon_4^{(3)} &= \frac{(r_y^2 + r_z^2)n_0 - r_y n_2 - r_z n_3}{r_m \sqrt{r_y^2 + r_z^2}}.
 \end{aligned} \tag{11}$$

Here, $E_1 = \sqrt{s x_1 x_2}/2$, $r_y = k_y/E_1$, $r_z = k_z/E_1$, $r_m = m_{B_c}/E_1$, and the on-shell (OS) condition constrains $r_y^2 + r_z^2 + r_m^2 = 1$. Then, the helicity amplitudes can be readily calculated through

$$\begin{aligned}
 \mathcal{M}_{\text{PP}}^{ij} &= A_{\text{PP}}^{\mu\nu} \epsilon_{1\mu}^{(i)} \epsilon_{2\nu}^{(j)}, \\
 \mathcal{M}_{\text{PV}}^{ijk} &= A_{\text{PV}}^{\mu\nu\rho} \epsilon_{1\mu}^{(i)} \epsilon_{2\nu}^{(j)} \epsilon_{3\rho}^{(k)}, \\
 \mathcal{M}_{\text{VP}}^{ijk} &= A_{\text{VP}}^{\mu\nu\rho} \epsilon_{1\mu}^{(i)} \epsilon_{2\nu}^{(j)} \epsilon_{4\rho}^{(k)}, \\
 \mathcal{M}_{\text{VV}}^{ijkl} &= A_{\text{VV}}^{\mu\nu\rho\sigma} \epsilon_{1\mu}^{(i)} \epsilon_{2\nu}^{(j)} \epsilon_{3\rho}^{(k)} \epsilon_{4\sigma}^{(l)}.
 \end{aligned} \tag{12}$$

The tree-level calculation is straightforward; however, the full analytic expressions of helicity amplitudes are still too lengthy to present in the main body of text. Considering the symmetric property in amplitudes, we present the LO results in the Appendix.

In the computation of one-loop amplitudes, the conventional dimensional regularization with $D = 4 - 2\epsilon$ is adopted to regularize the ultraviolet (UV) and infrared (IR) singularities. The IR singularities cancel each other and the UV singularities are removed by renormalization procedure. The renormalization constants include Z_2 , Z_m , Z_3 , and Z_g , corresponding to heavy quark field, heavy quark mass, gluon field, and strong coupling constant, respectively. We define Z_2 and Z_m in the OS scheme Z_3 and Z_g in the modified minimal-subtraction ($\overline{\text{MS}}$) scheme. The corresponding counterterms are

$$\begin{aligned}
 \delta Z_2^{\text{OS}} &= -C_F \frac{\alpha_s}{4\pi} \left[\frac{1}{\epsilon_{\text{UV}}} + \frac{2}{\epsilon_{\text{IR}}} - 3\gamma_E + 3 \ln \frac{4\pi\mu^2}{m^2} + 4 \right], \\
 \delta Z_m^{\text{OS}} &= -3C_F \frac{\alpha_s}{4\pi} \left[\frac{1}{\epsilon_{\text{UV}}} - \gamma_E + \ln \frac{4\pi\mu^2}{m^2} + \frac{4}{3} \right], \\
 \delta Z_3^{\overline{\text{MS}}} &= \frac{\alpha_s}{4\pi} (\beta_0 - 2C_A) \left[\frac{1}{\epsilon_{\text{UV}}} - \gamma_E + \ln(4\pi) \right], \\
 \delta Z_g^{\overline{\text{MS}}} &= -\frac{\beta_0}{2} \frac{\alpha_s}{4\pi} \left[\frac{1}{\epsilon_{\text{UV}}} - \gamma_E + \ln(4\pi) \right].
 \end{aligned} \tag{13}$$

Here, μ is the renormalization scale, γ_E is the Euler's constant; m stands for m_c and m_b accordingly; $\beta_0 = (11/3)C_A - (4/3)T_f n_f$ is the one-loop coefficient of QCD beta function, n_f is the number of active quarks which is taken to be 5 in our calculation; $C_A = 3$,

$C_F = 4/3$, and $T_F = 1/2$ are normal color factors. Note, in final results, all δZ_3 terms cancel with each other.

For reference, we provide the analytic results for one-loop amplitudes as Supplemental Material [34]. In the NLO calculation, the *Mathematica* package FeynArts [35] is used to generate Feynman diagrams and Feynman amplitudes; FeynCalc [36,37] and FORM [38,39] are used to perform algebraic calculation. The package FIRE [40,41] is employed to reduce the Feynman integrals to typical master integrals A_0 , B_0 , C_0 , and D_0 , which are numerically evaluated by LoopTools [42].

IV. NUMERICAL RESULTS

In numerical analysis, the formula (4) is employed with $|\mathcal{M}|^2 \simeq |\mathcal{M}_{\text{tree}}|^2$ for the LO calculation and $|\mathcal{M}|^2 \simeq |\mathcal{M}_{\text{tree}}|^2 + 2\text{Re}(\mathcal{M}_{\text{loop}}\mathcal{M}_{\text{tree}}^*)$ for the NLO calculation. The rapidity and p_T cuts, $|y| < 2$ and $2 < p_T < 40$ GeV, are imposed on each B_c meson. Other inputs in numerical evaluation go as follows:

$$\begin{aligned}
 \alpha &= 1/137.065, & m_e &= 0.511 \text{ MeV}, & m_c &= 1.5 \text{ GeV}, \\
 m_b &= 4.8 \text{ GeV}, & |\psi(0)|^2 &= 0.174 \text{ GeV}^3.
 \end{aligned} \tag{14}$$

Here, the B_c wave function at the origin is estimated from the ${}^3S_1 - {}^1S_0$ splitting [43],

$$|\psi(0)|^2 = \frac{9m_b m_c}{21\pi\alpha_s} (M_{B_c^*} - M_{B_c}), \tag{15}$$

with the lattice calculation result on $M_{B_c^*} - M_{B_c} = 53$ MeV [44].

The two-loop strong coupling of

$$\frac{\alpha_s(\mu)}{4\pi} = \frac{1}{\beta_0 L} - \frac{\beta_1 \ln L}{\beta_0^3 L^2} \tag{16}$$

is employed in the NLO calculation, in which, $L = \ln(\mu^2/\Lambda_{\text{QCD}}^2)$, $\beta_1 = (34/3)C_A^2 - 4C_F T_F n_f - (20/3)C_A T_F n_f$, with $n_f = 5$ and $\Lambda_{\text{QCD}} = 210$ MeV adopted here [45]. Note, for LO calculation, the one-loop formula of the running coupling constant is used.

Considering in future the e^+e^- collider like CEPC and ILC might run at center-of-mass energies $\sqrt{s} = 250$ GeV and $\sqrt{s} = 500$ GeV, respectively, we numerically evaluate the B_c -pair production via WWA and LBS schemes at these

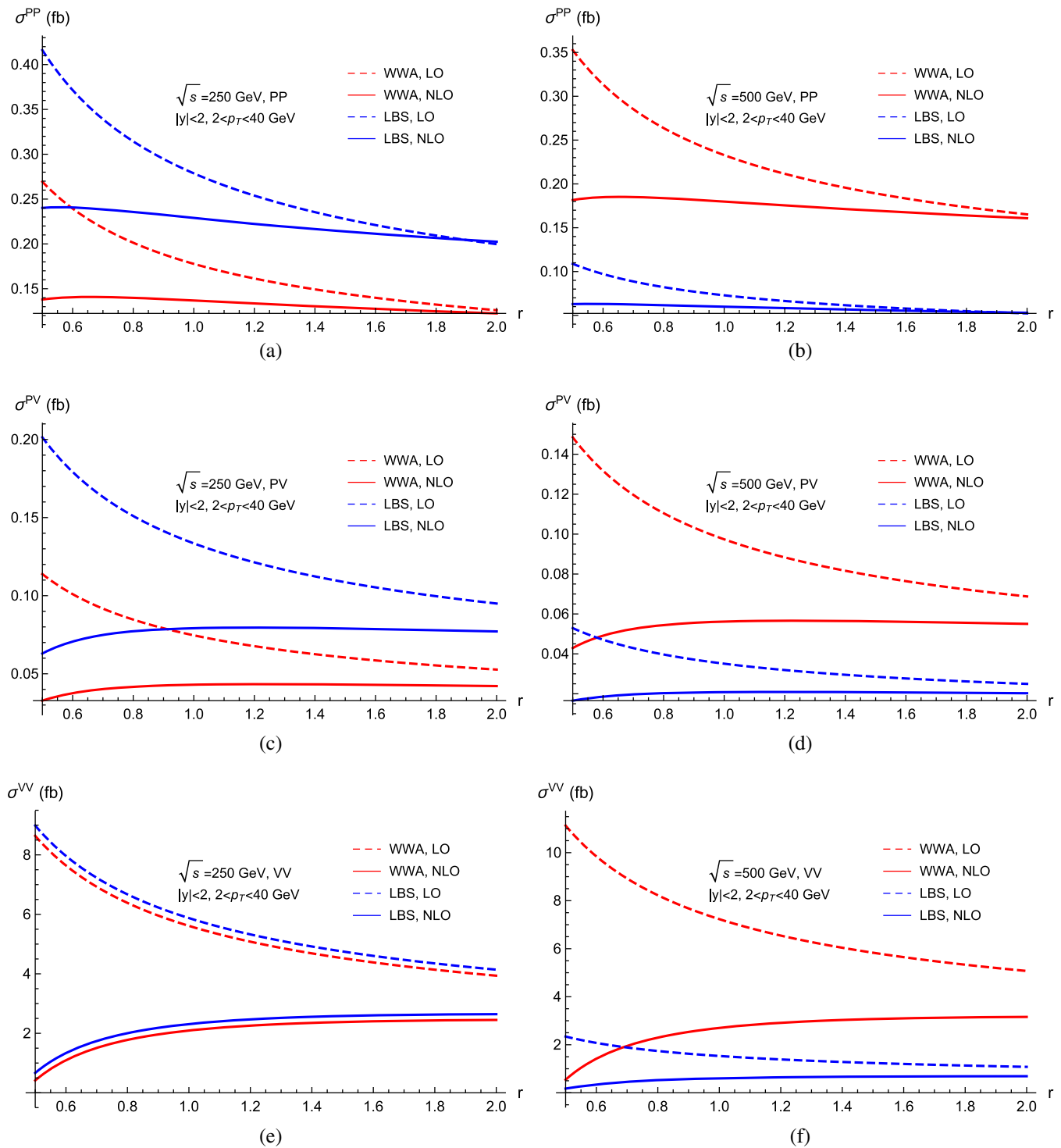


FIG. 3. The LO and NLO cross sections versus r , where $r = \frac{\mu}{\sqrt{m_{B_c}^2 + p_T^2}}$. (a) PP, 250 GeV; (b) PP, 500 GeV; (c) PV, 250 GeV; (d) PV, 500 GeV; (e) VV, 250 GeV; and (f) VV, 500 GeV.

two energies. Taking the same inputs, we can numerically repeat the LO double pseudoscalar B_c production result in [26]. The full NLO results are presented in Figs. 3–5. Note, because the cross sections for PV production and VP production are exactly the same, only the PV production results are illustrated.

The total cross sections versus r are shown in Fig. 3 with $\mu = r\sqrt{m_{B_c}^2 + p_T^2}$. We observe that, in comparison with the LO contribution, the LO plus NLO cross sections are suppressed, as are their dependences on the renormalization scale. As the \sqrt{s} rises from 250 to 500 GeV, the

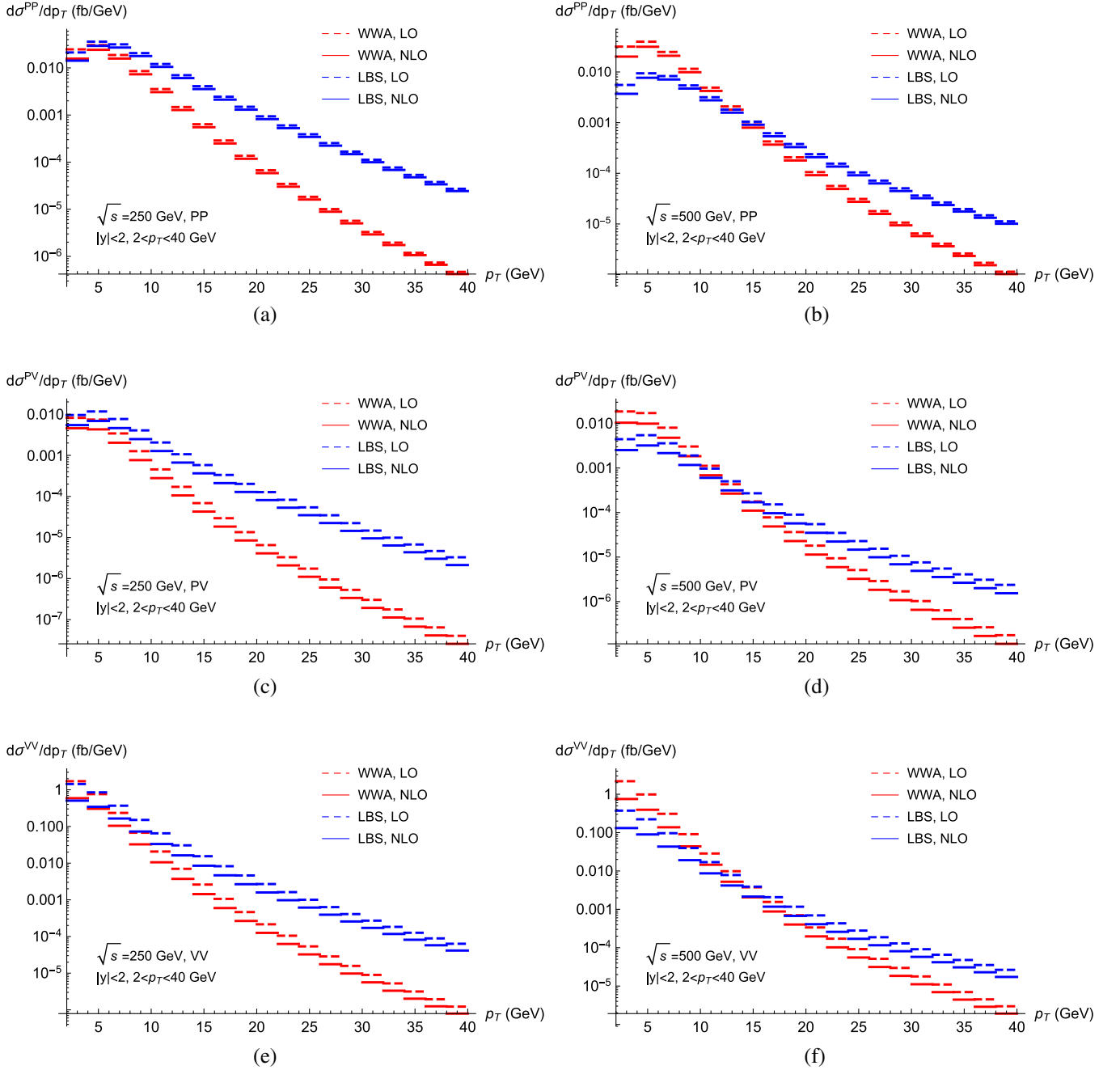


FIG. 4. The LO and NLO differential cross sections versus p_T , the transverse momentum of one of the two B_c mesons. The renormalization scale $\mu = \sqrt{m_{B_c}^2 + p_T^2}$. (a) PP, 250 GeV; (b) PP, 500 GeV; (c) PV, 250 GeV; (d) PV, 500 GeV; (e) VV, 250 GeV; and (f) VV, 500 GeV.

B_c -pair production rates increase in the WWA mechanism while decrease in the LBS mechanism. This may be understood from the different behaviors of WWA and LBS mechanisms, as shown in Fig. 1. The WWA photons are more likely to be produced with small momentum fraction x , while the LBS photons tend to be more energetic. Moreover, the partonic cross section $\hat{\sigma}(\gamma + \gamma \rightarrow B_c^+ + B_c^-)$ decreases with the increase of incident photons' center-of-mass energy.

The differential cross sections as functions of p_T , the transverse momentum of one of the two B_c mesons, are shown in Fig. 4. It can be seen that as \sqrt{s} increases from 250 to 500 GeV, the yields of WWA processes increase slightly, while the yields of LBS processes decrease, evidently in small p_T region. Since the LBS photons are generally more energetic than the WWA photons, the produced B_c pairs tend to have larger transverse momenta, which shall lead to a flatter p_T distribution.

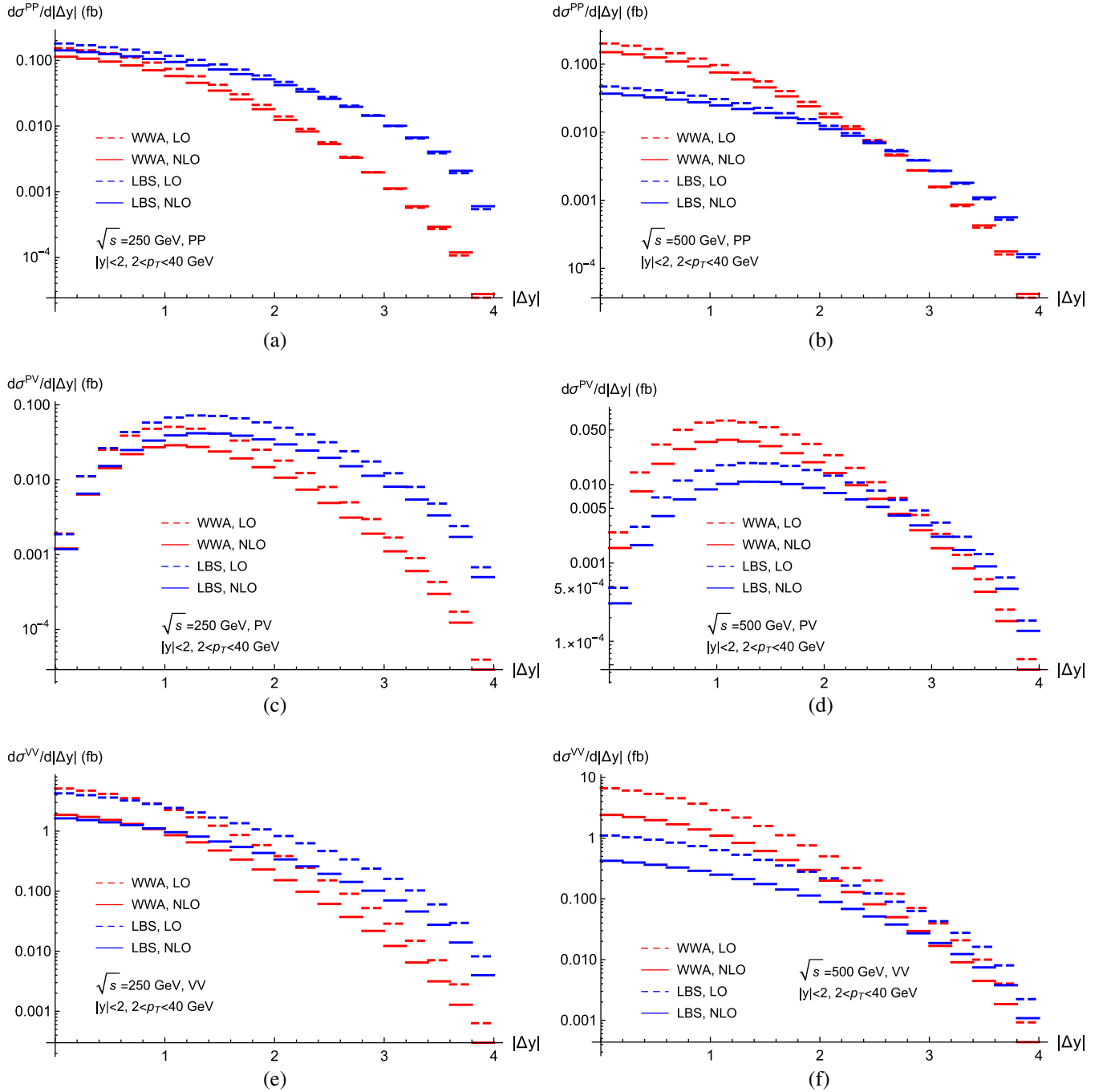


FIG. 5. The LO and NLO differential cross sections versus Δy , the rapidity difference between the two B_c mesons. The renormalization scale $\mu = \sqrt{m_{B_c}^2 + p_T^2}$. (a) PP, 250 GeV; (b) PP, 500 GeV; (c) PV, 250 GeV; (d) PV, 500 GeV; (e) VV, 250 GeV; and (f) VV, 500 GeV.

The differential cross sections as functions of Δy , the rapidity difference between two produced B_c mesons, are shown in Fig. 5. Note, due to $|\Delta y| = 2|y^*|$, the $|\Delta y|$ distribution is equivalent to the $|y^*|$ distribution, where y^* is the rapidity of B_c meson in the photon-photon center-of-mass frame. For PP and VV production, the B_c pairs are more likely to be produced around the $y^* = 0$ region, while for the PV or VP production, the peak is located

close to $y^* = 0.6$. Since the large energy may lead to large y^* , for the same reason as explained in p_T distribution, the LBS production distributions are flatter than the WWA ones.

In Ref. [30], the production of B_c pairs in e^+e^- annihilation via virtual γ^* and Z^* is investigated at the NLO QCD accuracy. At large \sqrt{s} , say $\sqrt{s} > 160$ GeV, the cross sections are less than 10^{-6} fb, which are 4–6 orders of magnitude smaller than the cross sections of the processes

considered here. It means that at high energy e^+e^- collider, photon-photon collision turns out to be the dominant mechanism for B_c -pair production.

Moreover, about the numerical results, there are some points remarkable which are as follows:

- (1) at $\sqrt{s} = 250$ GeV, as can be seen from Fig. 1, the WWA and LBS spectra meet at about $x \sim 0.07$, and hence the WWA and LBS cross sections tend to be comparable in the corresponding kinematic region (i.e., in about $2 < p_T < 4$ GeV and $0 < |\Delta y| < 1$), as shown in Figs. 4(a), 4(c), and 4(e) and Figs. 5(a), 5(c), and 5(e). For VV production, since small p_T and small $|\Delta y|$ regions dominate the production, the WWA and LBS cross sections are hence almost identical, as shown in Fig. 3(e).
- (2) To investigate the convergence of perturbative expansion, we define a measure $\mathcal{R} = \left| \frac{\sigma_{\text{NLO}} - \sigma_{\text{LO}}}{\sigma_{\text{LO}}} \right|$. For PP, PV, and VV productions, we find

$$\begin{aligned} 0 < \mathcal{R}_{\text{PP}} < 0.5, \quad 0.2 < \mathcal{R}_{\text{PV}} < 0.7, \\ 0.4 < \mathcal{R}_{\text{VV}} < 0.9, \end{aligned} \quad (17)$$

which are compatible with the results in Ref. [30], where the B_c -pair production via e^+e^- annihilation was studied. Furthermore, the NLO effect is more significant in the small p_T region, suggests a resummation for the logarithms of $\frac{p_T^2}{s}$, which is beyond the scope of this work.

- (3) In the numerical calculation, the strong coupling constant is parametrized by Λ_{QCD} as in Eq. (16). However, it is noteworthy that nowadays an alternative approach is widely accepted, in which the initial value of α_s at a well-experimentally measured point is adopted, usually at M_Z , rather than Λ_{QCD} . Then, for fixed n_f , one may use evolution equation [46]

$$\begin{aligned} \frac{4\pi}{\alpha_s(\mu^2)} - \frac{\beta_1}{\beta_0} \ln \left(\frac{4\pi}{\alpha_s(\mu^2)} + \frac{\beta_1}{\beta_0} \right) \\ = \frac{4\pi}{\alpha_s(M_Z^2)} - \frac{\beta_1}{\beta_0} \ln \left(\frac{4\pi}{\alpha_s(M_Z^2)} + \frac{\beta_1}{\beta_0} \right) + \beta_0 \ln \frac{\mu^2}{M_Z^2} \end{aligned} \quad (18)$$

to run the α_s to where interested in. We evaluate the cross sections as well employing this parametrizing scheme with input $\alpha_s(M_Z^2) = 0.1181$ [45] and find that in comparison with the results from the original scheme, the LO cross sections are generally suppressed substantially by a factor of about 0.7, while the dominance of the NLO results in two schemes alternates case to case, but with discrepancies less than 5%. As a good approximation, to match to the evolution scheme, one may keep on using Eq. (16), but with Λ_{QCD} determined by $\alpha_s(M_Z^2)$, i.e., $\Lambda_{\text{QCD}}^{\text{LO}} = 88$ MeV, $\Lambda_{\text{QCD}}^{\text{NLO}} = 228$ MeV. In all, the discrepancy in strong coupling constant parametrization between two schemes

may be somehow remedied by adjusting the value of Λ_{QCD} , but the evolution scheme is recommended.

V. SUMMARY

In this work, we investigated the B_c -pair production in high energy photon-photon fusion at the NLO accuracy in the NRQCD factorization framework. Various of S -wave B_c states, including configurations of PP, PV, VP, and VV, were taken into account. Considering the leading order results for B_c -pair production in PV and VP configurations are still missing in the literature, we calculated them and provided the analytic results. The total cross section and p_T and Δy distributions in e^+e^- collider with $\sqrt{s} = 250$ GeV and $\sqrt{s} = 500$ GeV were evaluated and presented in figures.

The numerical results show that with the NLO corrections, the LO cross sections are suppressed, and their dependence on renormalization scale is reduced evidently. By comparing with the results in Ref. [30], where the B_c -pair production in e^+e^- annihilation via virtual γ^* and Z^* was investigated, we may conclude that at large e^+e^- collision energy, say $\sqrt{s} > 160$ GeV, photon-photon collision will be the dominant source of B_c -pair production.

The NLO calculation of the concerned processes is somewhat time consuming and computer resource exhausting. To fulfill this work, a “divide-and-conquer” strategy was employed. Instead of squaring the amplitude and summing over spins, we calculated the helicity amplitudes separately, which makes this tedious calculation workable. Moreover, it shows that the symmetries remain in the helicity amplitudes may greatly reduce the number of independent amplitudes, as illustrated in the Appendix.

Last, the concerned processes involve a number of momenta and polarization vectors of the external particles, by introducing auxiliary vectors, the base n_0, n_1, n_2 , and n_3 , the number of independent Lorentz vectors reduces to 4, which facilitate the computation of Feynman integrals. We think the technical strategy employed in this work might be applicable to the studies of some other relevant processes.

ACKNOWLEDGMENTS

This work was supported in part by the National Natural Science Foundation of China under Grants No. 11975236 and No. 11635009.

Note added.—When this work was finished and the paper was finalizing, there appeared a study on the web about the B_c -pair production in photon-photon collision with the relativistic corrections [47].

APPENDIX: TREE-LEVEL HELICITY AMPLITUDES

For PP, PV (or VP), and VV production, there are 4, 12, and 36 helicity amplitudes, respectively, whereas half of them are zero. The nonzero helicity amplitudes are

$$\begin{aligned}
 & \mathcal{M}_{\text{PP}}^{11}, \mathcal{M}_{\text{PP}}^{44}, \mathcal{M}_{\text{PV,VP}}^{111}, \mathcal{M}_{\text{PV,VP}}^{122}, \mathcal{M}_{\text{PV,VP}}^{123}, \mathcal{M}_{\text{PV,VP}}^{212}, \mathcal{M}_{\text{PV,VP}}^{213}, \\
 & \mathcal{M}_{\text{PV,VP}}^{221}, \mathcal{M}_{\text{VV}}^{1111}, \mathcal{M}_{\text{VV}}^{1122}, \mathcal{M}_{\text{VV}}^{1123}, \mathcal{M}_{\text{VV}}^{1132}, \mathcal{M}_{\text{VV}}^{1133}, \mathcal{M}_{\text{VV}}^{1212}, \\
 & \mathcal{M}_{\text{VV}}^{1213}, \mathcal{M}_{\text{VV}}^{1221}, \mathcal{M}_{\text{VV}}^{1231}, \mathcal{M}_{\text{VV}}^{2112}, \mathcal{M}_{\text{VV}}^{2113}, \mathcal{M}_{\text{VV}}^{2121}, \mathcal{M}_{\text{VV}}^{2131}, \\
 & \mathcal{M}_{\text{VV}}^{2211}, \mathcal{M}_{\text{VV}}^{2222}, \mathcal{M}_{\text{VV}}^{2223}, \mathcal{M}_{\text{VV}}^{2232}, \mathcal{M}_{\text{VV}}^{2233}. \quad (\text{A1})
 \end{aligned}$$

The processes of PV and VP productions are correlated in charge-conjugation transformation; their cross sections should be exactly the same. According convention (10) and (11), the amplitudes satisfy

$$\mathcal{M}_{\text{PV}}^{ijk} = \pm \mathcal{M}_{\text{VP}}^{ijk}, \quad (\text{A2})$$

where the plus sign corresponds to $\{i, j, k\} = \{1, 1, 1\}$ and $\{2, 2, 1\}$, and the minus sign corresponds to other cases. In addition, the helicity amplitudes satisfy also

$$\begin{aligned}
 \mathcal{M}_{\text{PV}}^{122} &= \mathcal{M}_{\text{PV}}^{212}|_{k_z \rightarrow -k_z}, & \mathcal{M}_{\text{PV}}^{123} &= -\mathcal{M}_{\text{PV}}^{213}|_{k_z \rightarrow -k_z}, \\
 \mathcal{M}_{\text{VP}}^{122} &= \mathcal{M}_{\text{VP}}^{212}|_{k_z \rightarrow -k_z}, & \mathcal{M}_{\text{VP}}^{123} &= -\mathcal{M}_{\text{VP}}^{213}|_{k_z \rightarrow -k_z}, \\
 \mathcal{M}_{\text{VV}}^{1123} &= -\mathcal{M}_{\text{VV}}^{1132}, & \mathcal{M}_{\text{VV}}^{2223} &= -\mathcal{M}_{\text{VV}}^{2232}, \\
 \mathcal{M}_{\text{VV}}^{1212} &= -\mathcal{M}_{\text{VV}}^{1221}|_{k_z \rightarrow -k_z} = -\mathcal{M}_{\text{VV}}^{2112}|_{k_z \rightarrow -k_z} = \mathcal{M}_{\text{VV}}^{2121}, \\
 \mathcal{M}_{\text{VV}}^{1213} &= -\mathcal{M}_{\text{VV}}^{1231}|_{k_z \rightarrow -k_z} = \mathcal{M}_{\text{VV}}^{2113}|_{k_z \rightarrow -k_z} = -\mathcal{M}_{\text{VV}}^{2131}. \quad (\text{A3})
 \end{aligned}$$

The analytical expressions for helicity amplitudes can be classified in photon-quark coupling as

$$\begin{aligned}
 \mathcal{M} &= \frac{8C_A C_F m_{B_c}^3 \pi^2 \alpha \alpha_s}{3E_1^2 m_b^2 m_c^2} \\
 &\times \left[e_c^2 f_1 - e_c e_b (f_2 + f_3) + e_b^2 f_4 + \sum_{i=u,d,s} e_i^2 f_5 \right], \quad (\text{A4})
 \end{aligned}$$

where e_q represents the electric charge number of quark q , i.e., $e_c = e_u = \frac{2}{3}$, $e_d = e_s = e_b = -\frac{1}{3}$. The coefficients f_1 and f_4 , f_2 and f_3 are related as per $m_c \leftrightarrow m_b$ exchange,

$$\begin{aligned}
 f_{\text{PP},1}|_{m_c \leftrightarrow m_b} &= f_{\text{PP},4}, & f_{\text{PP},2}|_{m_c \leftrightarrow m_b} &= f_{\text{PP},3}, \\
 f_{\text{PV},1}|_{m_c \leftrightarrow m_b} &= -f_{\text{PV},4}, & f_{\text{PV},2}|_{m_c \leftrightarrow m_b} &= -f_{\text{PV},3}, \\
 f_{\text{VP},1}|_{m_c \leftrightarrow m_b} &= -f_{\text{VP},4}, & f_{\text{VP},2}|_{m_c \leftrightarrow m_b} &= -f_{\text{VP},3}, \\
 f_{\text{VV},1}|_{m_c \leftrightarrow m_b} &= f_{\text{VV},4}, & f_{\text{VV},2}|_{m_c \leftrightarrow m_b} &= f_{\text{VV},3}. \quad (\text{A5})
 \end{aligned}$$

For the tree amplitudes, f_5 is zero. The analytical results for other coefficients are

$$\begin{aligned}
 f_{\text{PP},4}^{11} &= -\frac{r^2(1-r_z^2)}{r-1} - \frac{r_y^2}{(r-1)(1-r_z^2)} + \frac{r(rr_y^2-2r+3)}{r-1} - \frac{2r_y^2}{(1-r_z^2)^2}, \\
 f_{\text{PP},3}^{11} &= 1 - \frac{2r_y^2}{(1-r_z^2)^2}, \\
 f_{\text{PP},4}^{22} &= -\frac{2r_y^2(2r^2r_y^2-4r^2+4r-1)}{(1-r_z^2)^2} - \frac{r^2(1-r_z^2)}{r-1} + \frac{r_y^2(4r^3-2r^2r_y^2-6r+1)}{(r-1)(1-r_z^2)} + \frac{r(3rr_y^2-2r+3)}{r-1}, \\
 f_{\text{PP},3}^{22} &= \frac{2(2r^2-2r-1)r_y^2}{1-r_z^2} - \frac{2r_y^2(2r^2r_y^2-4r^2-2rr_y^2+4r-1)}{(1-r_z^2)^2} + 1; \\
 f_{\text{PV},4}^{111} &= ir_m r_y r_z \left(\frac{r}{(r-1)(1-r_z^2)} + \frac{2}{(1-r_z^2)^2} \right), \\
 f_{\text{PV},3}^{111} &= -\frac{i2r_m r_y r_z}{(1-r_z^2)^2}, \\
 f_{\text{PV},4}^{122} &= \frac{ir_m r_y}{\sqrt{r_y^2+r_z^2}} \left(\frac{2r^2+rr_y^2-3r+2}{(r-1)(1-r_z^2)} + \frac{2(rr_y^2+rr_z-r+1)}{(1-r_z^2)^2} - \frac{r}{r-1} \right), \\
 f_{\text{PV},3}^{122} &= \frac{ir_m r_y}{\sqrt{r_y^2+r_z^2}} \left(\frac{2(rr_y^2+rr_z-r-r_y^2-r_z)}{(1-r_z^2)^2} + \frac{2r}{1-r_z^2} \right), \\
 f_{\text{PV},4}^{123} &= \frac{i}{\sqrt{r_y^2+r_z^2}} \left(-\frac{rr_y^2(2r-r_y^2-3)}{(r-1)(1-r_z^2)} + \frac{2r_y^2(rr_y^2+2rr_z-r_z)}{(1-r_z^2)^2} - \frac{r(2r_y^2+1)}{r-1} + \frac{r(1-r_z^2)}{r-1} \right),
 \end{aligned}$$

$$\begin{aligned}
f_{\text{PV},3}^{123} &= \frac{i}{\sqrt{r_y^2 + r_z^2}} \left(\frac{2(rr_y^2 + 2rr_z - r_y^2 - r_z)}{(1 - r_z^2)^2} - \frac{2(r-1)}{1 - r_z^2} \right), \\
f_{\text{PV},4}^{221} &= ir_m r_y r_z \left(\frac{2(2r-1)}{(1 - r_z^2)^2} - \frac{r}{(r-1)(1 - r_z^2)} \right), \\
f_{\text{PV},3}^{221} &= i2r_m r_y r_z \frac{-1 + 2r}{(1 - r_z^2)^2}, \\
f_{\text{VV},4}^{1111} &= \frac{r^2(1 - r_z^2)}{r-1} - \frac{2r - r_y^2 - 2}{(r-1)(1 - r_z^2)} - \frac{r(rr_y^2 + 1)}{r-1} + \frac{2r_y^2}{(1 - r_z^2)^2}, \\
f_{\text{VV},3}^{1111} &= -\frac{2r_y^2}{(1 - r_z^2)^2} + \frac{2}{1 - r_z^2} - 1, \\
f_{\text{VV},4}^{1122} &= \frac{1}{r_y^2 + r_z^2} \left(-\frac{r^2 r_y^4 + r^2 r_y^2 + rr_y^2 + 3r + r_y^2 - 2}{r-1} - \frac{r^2(1 - r_z^2)^2}{r-1} + \frac{r(1 - r_z^2)(2rr_y^2 + r + 1)}{r-1} \right. \\
&\quad \left. + \frac{(r_y^2 + 1)(2r + r_y^2 - 2)}{(r-1)(1 - r_z^2)} + \frac{2(r_y - 1)(r_y + 1)r_y^2}{(1 - r_z^2)^2} \right), \\
f_{\text{VV},3}^{1122} &= \frac{1}{r_y^2 + r_z^2} \left(-\frac{2r_y^2}{(1 - r_z^2)^2} + \frac{2(2r_y^2 + 1)}{1 - r_z^2} - r_y^2 - r_z^2 - 2 \right), \\
f_{\text{VV},4}^{1123} &= \frac{r_m r_y r_z}{r_y^2 + r_z^2} \left(\frac{r(r_y^2 + 1)}{(r-1)(1 - r_z^2)} - \frac{r}{r-1} + \frac{2(r_y - 1)(r_y + 1)}{(1 - r_z^2)^2} \right), \\
f_{\text{VV},3}^{1123} &= \frac{r_m r_y r_z}{r_y^2 + r_z^2} \left(\frac{2}{1 - r_z^2} - \frac{2}{(1 - r_z^2)^2} \right), \\
f_{\text{VV},4}^{1133} &= \frac{1}{r_y^2 + r_z^2} \left(-\frac{r^2 r_y^4 + 3r^2 r_y^2 + 2r^2 - rr_y^2 - r + r_y^2}{r-1} - \frac{r^2(1 - r_z^2)^2}{r-1} + \frac{(r_y^2 + 1)r_y^2}{(r-1)(1 - r_z^2)} \right. \\
&\quad \left. + \frac{r(1 - r_z^2)(2rr_y^2 + 3r - 1)}{r-1} + \frac{2(r_y - 1)(r_y + 1)r_y^2}{(1 - r_z^2)^2} \right), \\
f_{\text{VV},3}^{1133} &= \frac{1}{r_y^2 + r_z^2} \left(\frac{2r_y^2}{1 - r_z^2} - \frac{2r_y^2}{(1 - r_z^2)^2} - r_y^2 - r_z^2 \right), \\
f_{\text{VV},4}^{1212} &= \frac{r_m^2}{\sqrt{r_y^2 + r_z^2}} \left(-\frac{r(r_y^2 + 1)}{(r-1)(1 - r_z^2)} - \frac{2(rr_y^2 + r_z)}{(1 - r_z^2)^2} + \frac{r}{r-1} \right), \\
f_{\text{VV},3}^{1212} &= \frac{r_m^2}{\sqrt{r_y^2 + r_z^2}} \left(-\frac{2(rr_y^2 - r_y^2 - 1)}{(1 - r_z^2)^2} - \frac{2}{1 - r_z^2} \right), \\
f_{\text{VV},4}^{1213} &= \frac{r_m r_y}{\sqrt{r_y^2 + r_z^2}} \left(\frac{r(2r - r_y^2 - 3)}{(r-1)(1 - r_z^2)} - \frac{2(rr_y^2 + rr_z + r - 1)}{(1 - r_z^2)^2} + \frac{r}{r-1} \right), \\
f_{\text{VV},3}^{1213} &= \frac{r_m r_y}{\sqrt{r_y^2 + r_z^2}} \left(\frac{2(r-1)}{1 - r_z^2} - \frac{2(rr_y^2 + rr_z + r - r_y^2 - 1)}{(1 - r_z^2)^2} \right), \\
f_{\text{VV},4}^{2211} &= \frac{2r_y^2(2r^2 r_y^2 - 1)}{(1 - r_z^2)^2} + \frac{r^2(1 - r_z^2)}{r-1} - \frac{4r^3 r_y^2 - 2r^2 r_y^4 - 4r^2 r_y^2 - 2rr_y^2 - 2r + r_y^2 + 2}{(r-1)(1 - r_z^2)} - \frac{r(3rr_y^2 + 1)}{r-1}, \\
f_{\text{VV},3}^{2211} &= \frac{2r_y^2(2r^2 r_y^2 - 2rr_y^2 - 1)}{(1 - r_z^2)^2} - \frac{2(2r^2 r_y^2 - 2rr_y^2 - r_y^2 - 1)}{1 - r_z^2} - 1,
\end{aligned}$$

$$\begin{aligned}
f_{\text{VV},4}^{2222} &= \frac{1}{r_y^2 + r_z^2} \left(\frac{2r_y^2(2r^2r_y^4 + 2r^2r_y^2 - r_y^2 + 1)}{(1 - r_z^2)^2} - \frac{r^2(1 - r_z^2)^2}{r - 1} + \frac{4r^3r_y^2 - 5r^2r_y^4 - 7r^2r_y^2 - 3rr_y^2 + r + r_y^2 - 2}{r - 1} \right. \\
&\quad \left. - \frac{8r^3r_y^4 + 4r^3r_y^2 - 2r^2r_y^6 - 10r^2r_y^4 - 4r^2r_y^2 - 2rr_y^4 + 2r + r_y^4 - r_y^2 - 2}{(r - 1)(1 - r_z^2)} + \frac{r(1 - r_z^2)(4rr_y^2 + r + 1)}{r - 1} \right), \\
f_{\text{VV},3}^{2222} &= \frac{1}{r_y^2 + r_z^2} \left(\frac{2r_y^2(2r^2r_y^4 + 2r^2r_y^2 - 2rr_y^4 - 2rr_y^2 - 2r_y^2 - 1)}{(1 - r_z^2)^2} - \frac{2(4r^2r_y^4 + 2r^2r_y^2 - 4rr_y^4 - 2rr_y^2 - r_y^4 - 3r_y^2 - 1)}{1 - r_z^2} \right. \\
&\quad \left. \times 4r^2r_y^2 + -4rr_y^2 - 3r_y^2 - r_z^2 - 2 \right), \\
f_{\text{VV},4}^{2223} &= \frac{r_m r_y r_z}{r_y^2 + r_z^2} \left(\frac{r(4r - r_y^2 - 5)}{(r - 1)(1 - r_z^2)} - \frac{2(2rr_y^2 + 2r + r_y^2 - 1)}{(1 - r_z^2)^2} + \frac{r}{r - 1} \right), \\
f_{\text{VV},3}^{2223} &= \frac{r_m r_y r_z}{\sqrt{r_y^2 + r_z^2}} \left(\frac{2(2r - 1)}{1 - r_z^2} - \frac{2(2rr_y^2 + 2r + r_y^2 r_z - r_y^2 - 1)}{(1 - r_z^2)^2} \right), \\
f_{\text{VV},4}^{2233} &= \frac{1}{r_y^2 + r_z^2} \left(\frac{2r_y^2(2r^2r_y^4 + 6r^2r_y^2 + 4r^2 - 4rr_y^2 - 4r - r_y^2 + 1)}{(1 - r_z^2)^2} - \frac{r^2(1 - r_z^2)^2}{r - 1} + \frac{r(1 - r_z^2)(4rr_y^2 + 3r - 1)}{r - 1} \right. \\
&\quad \left. - \frac{r_y^2(8r^3r_y^2 + 12r^3 - 2r^2r_y^4 - 14r^2r_y^2 - 24r^2 + 2rr_y^2 + 10r + r_y^2 + 1)}{(r - 1)(1 - r_z^2)} \right. \\
&\quad \left. + \frac{4r^3r_y^2 - 5r^2r_y^4 - 13r^2r_y^2 - 2r^2 + 3rr_y^2 + r + r_y^2}{r - 1} \right), \\
f_{\text{VV},3}^{2233} &= \frac{1}{r_y^2 + r_z^2} \left(- \frac{2r_y^2(4r^2r_y^2 + 6r^2 - 4rr_y^2 - 6r - r_y^2)}{1 - r_z^2} + \frac{2r_y^2(2r^2r_y^4 + 6r^2r_y^2 + 4r^2 - 2rr_y^4 - 6rr_y^2 - 4r + 1)}{(1 - r_z^2)^2} \right. \\
&\quad \left. + 4r^2r_y^2 - 4rr_y^2 - 3r_y^2 - r_z^2 \right). \tag{A6}
\end{aligned}$$

Here, $r = m_b/(m_b + m_c)$. The analytical results for the one-loop amplitude are lengthy and are presented in the Supplemental Material [34].

-
- | | |
|---|---|
| [1] F. Abe <i>et al.</i> (CDF Collaboration), <i>Phys. Rev. Lett.</i> 81 , 2432 (1998). | [10] Z. Yang, X. G. Wu, and X. Y. Wang, <i>Comput. Phys. Commun.</i> 184 , 2848 (2013). |
| [2] F. Abe <i>et al.</i> (CDF Collaboration), <i>Phys. Rev. D</i> 58 , 112004 (1998). | [11] X. C. Zheng, C. H. Chang, T. F. Feng, and Z. Pan, <i>Sci. China Phys. Mech. Astron.</i> 61 , 031012 (2018). |
| [3] G. Aad <i>et al.</i> (ATLAS Collaboration), <i>Phys. Rev. Lett.</i> 113 , 212004 (2014). | [12] A. Berezhnoy, A. Likhoded, and M. Shevlyagin, <i>Phys. Lett. B</i> 342 , 351 (1995). |
| [4] A. M. Sirunyan <i>et al.</i> (CMS Collaboration), <i>Phys. Rev. Lett.</i> 122 , 132001 (2019). | [13] K. Kolodziej, A. Leike, and R. Ruckl, <i>Phys. Lett. B</i> 348 , 219 (1995). |
| [5] G. T. Bodwin, E. Braaten, and G. Lepage, <i>Phys. Rev. D</i> 51 , 1125 (1995); 55 , 5853(E) (1997). | [14] A. Berezhnoy, V. Kiselev, and A. Likhoded, <i>Phys. At. Nucl.</i> 61 , 252 (1998). |
| [6] C. H. Chang and Y. Q. Chen, <i>Phys. Rev. D</i> 48 , 4086 (1993). | [15] H. Y. Bi, R. Y. Zhang, H. Y. Han, Y. Jiang, and X. G. Wu, <i>Phys. Rev. D</i> 95 , 034019 (2017). |
| [7] C. H. Chang, Y. Q. Chen, G. P. Han, and H. T. Jiang, <i>Phys. Lett. B</i> 364 , 78 (1995). | [16] C. F. Qiao, C. S. Li, and K. T. Chao, <i>Phys. Rev. D</i> 54 , 5606 (1996). |
| [8] A. Berezhnoy, A. Likhoded, and O. Yushchenko, <i>Phys. At. Nucl.</i> 59 , 709 (1996). | [17] P. Sun, L. P. Sun, and C. F. Qiao, <i>Phys. Rev. D</i> 81 , 114035 (2010). |
| [9] K. Kolodziej, A. Leike, and R. Ruckl, <i>Phys. Lett. B</i> 355 , 337 (1995). | [18] C. H. Chang and Y. Q. Chen, <i>Phys. Rev. D</i> 46 , 3845 (1992); 50 , 6013(E) (1994). |

- [19] V. Kiselev, A. Likhoded, and M. Shevlyagin, *Phys. At. Nucl.* **57**, 689 (1994).
- [20] C. F. Qiao, L. P. Sun, and R. L. Zhu, *J. High Energy Phys.* **08** (2011) 131.
- [21] J. Jiang, L. B. Chen, and C. F. Qiao, *Phys. Rev. D* **91**, 034033 (2015).
- [22] C. F. Qiao, L. P. Sun, D. S. Yang, and R. L. Zhu, *Eur. Phys. J. C* **71**, 1766 (2011).
- [23] X. C. Zheng, C. H. Chang, X. G. Wu, J. Zeng, and X. D. Huang, *Phys. Rev. D* **101**, 034029 (2020).
- [24] Z. Q. Chen, H. Yang, and C. F. Qiao, *Phys. Rev. D* **101**, 036009 (2020).
- [25] J. Jiang and C. F. Qiao, *Phys. Rev. D* **93**, 054031 (2016).
- [26] S. Baranov, *Phys. Rev. D* **55**, 2756 (1997).
- [27] R. Li, Y. J. Zhang, and K. T. Chao, *Phys. Rev. D* **80**, 014020 (2009).
- [28] V. Kiselev, *Int. J. Mod. Phys. A* **10**, 465 (1995).
- [29] A. Karyasov, A. Martynenko, and F. Martynenko, *Nucl. Phys.* **B911**, 36 (2016).
- [30] A. Berezhnoy, A. Likhoded, A. Onishchenko, and S. Poslavsky, *Nucl. Phys.* **B915**, 224 (2017).
- [31] S. Frixione, M. L. Mangano, P. Nason, and G. Ridolfi, *Phys. Lett. B* **319**, 339 (1993).
- [32] I. Ginzburg, G. Kotkin, V. Serbo, and V. I. Telnov, *Nucl. Instrum. Methods* **205**, 47 (1983).
- [33] V. I. Telnov, *Nucl. Instrum. Methods Phys. Res., Sect. A* **294**, 72 (1990).
- [34] See Supplemental Material at <http://link.aps.org/supplemental/10.1103/PhysRevD.102.016011> for analytical results for the one-loop helicity amplitudes.
- [35] T. Hahn, *Comput. Phys. Commun.* **140**, 418 (2001).
- [36] R. Mertig, M. Bohm, and A. Denner, *Comput. Phys. Commun.* **64**, 345 (1991).
- [37] V. Shtabovenko, R. Mertig, and F. Orellana, *Comput. Phys. Commun.* **207**, 432 (2016).
- [38] J. Vermaseren, *Nucl. Phys. B, Proc. Suppl.* **183**, 19 (2008).
- [39] J. Kuipers, T. Ueda, J. Vermaseren, and J. Vollinga, *Comput. Phys. Commun.* **184**, 1453 (2013).
- [40] A. Smirnov, *J. High Energy Phys.* **10** (2008) 107.
- [41] A. V. Smirnov, *Comput. Phys. Commun.* **189**, 182 (2015).
- [42] T. Hahn and M. Perez-Victoria, *Comput. Phys. Commun.* **118**, 153 (1999).
- [43] E. J. Eichten and C. Quigg, *Phys. Rev. D* **49**, 5845 (1994).
- [44] E. B. Gregory, C. T. H. Davies, I. D. Kendall, J. Koponen, K. Wong, E. Follana, E. Gamiz, G. P. Lepage, E. H. Muller, H. Na, and J. Shigemitsu, *Phys. Rev. D* **83**, 014506 (2011).
- [45] M. Tanabashi *et al.* (Particle Data Group), *Phys. Rev. D* **98**, 030001 (2018).
- [46] A. Deur, S. J. Brodsky, and G. F. de Teramond, *Prog. Part. Nucl. Phys.* **90**, 1 (2016).
- [47] A. E. Dorokhov, R. N. Faustov, A. P. Martynenko, and F. A. Martynenko, [arXiv:2005.06053](https://arxiv.org/abs/2005.06053).